The Biosynthetic Pathway of Indole-3-Carbaldehyde and Indole-3-Carboxylic Acid Derivatives in Arabidopsis[1][W]

Christoph Böttcher[2], Alexandra Chapman, Franziska Fellermeier, Manisha Choudhary, Dierk Scheel, and Erich Glawischnig*

Leibniz Institute of Plant Biochemistry, Department of Stress and Developmental Biology, 06120 Halle/Saale, Germany (C.B., D.S.); and Lehrstuhl für Genetik, Technische Universität München, 85354 Freising, Germany (A.C., F.F., M.C., E.G.)

Indolic secondary metabolites play an important role in pathogen defense in cruciferous plants. In Arabidopsis (*Arabidopsis thaliana*), in addition to the characteristic phytoalexin camalexin, derivatives of indole-3-carbaldehyde (ICHO) and indole-3-carboxylic acid (ICOOH) are synthesized from tryptophan via the intermediates indole-3-acetaldoxime and indole-3-acetonitrile. Based on feeding experiments combined with nontargeted metabolite profiling, their composition in nontreated and silver nitrate ($AgNO_3$)-treated leaf tissue was comprehensively analyzed. As major derivatives, glucose conjugates of 5-hydroxyindole-3-carbaldehyde, ICOOH, and 6-hydroxyindole-3-carboxylic acid were identified. Quantification of ICHO and ICOOH derivative pools after glucosidase treatment revealed that, in response to $AgNO_3$ treatment, their total accumulation level was similar to that of camalexin. *ARABIDOPSIS ALDEHYDE OXIDASE1* (*AAO1*), initially discussed to be involved in the biosynthesis of indole-3-acetic acid, and *Cytochrome P450* (*CYP*) *71B6* were found to be transcriptionally coexpressed with camalexin biosynthetic genes. CYP71B6 was expressed in *Saccharomyces cerevisiae* and shown to efficiently convert indole-3-acetonitrile into ICHO and ICOOH, thereby releasing cyanide. To evaluate the role of both enzymes in the biosynthesis of ICHO and ICOOH derivatives, knockout and overexpression lines for *CYP71B6* and *AAO1* were established and analyzed for indolic metabolites. The observed metabolic phenotypes suggest that AAO1 functions in the oxidation of ICHO to ICOOH in both nontreated and $AgNO_3$-treated leaves, whereas CYP71B6 is relevant for ICOOH derivative biosynthesis specifically after induction. In summary, a model for the biosynthesis of ICHO and ICOOH derivatives is presented.

Essential for the fitness of plants in their environment is their capability to synthesize secondary metabolites involved in defense against pathogens and herbivores. Typical for the Brassicaceae is the formation of Trp-derived indole glucosinolates and indolic phytoalexins (Sønderby et al., 2010; Pedras et al., 2011). In Arabidopsis (*Arabidopsis thaliana*), mainly 1-methoxy-, 4-methoxy, and unmodified indol-3-ylmethyl glucosinolate (IMG) constitutively accumulate as major Trp-derived phytoanticipins. In addition, 4-methoxy-IMG biosynthesis is stimulated upon microbial attack, and its degradation products contribute to resistance to a number of fungal pathogens (Bednarek et al., 2009; Clay et al., 2009). The first step in indole glucosinolate biosynthesis is the formation of indole-3-acetaldoxime (IAOx) from Trp by Cytochrome P450 (CYP)79B2 and CYP79B3 (Hull et al., 2000; Mikkelsen et al., 2000; Zhao et al., 2002). This step is shared with the biosynthesis of a number of metabolites whose accumulation is induced upon infection or silver nitrate ($AgNO_3$) treatment and that are absent in IAOx-deficient *cyp79B2 cyp79B3* mutant plants (Glawischnig et al., 2004; Böttcher et al., 2009). Here, camalexin is the prominent compound (Rauhut and Glawischnig, 2009). It is synthesized from IAOx via indole-3-acetonitrile (IAN), from which a glutathione conjugate is formed (Geu-Flores et al., 2011; Su et al., 2011; Møldrup et al., 2013). This is then degraded to a cysteine-indole-3-acetonitrile conjugate [Cys(IAN)], the substrate of a unique bifunctional P450 monooxygenase, CYP71B15 (PHYTOALEXIN-DEFICIENT3 [PAD3]; Zhou et al., 1999; Schuhegger et al., 2006; Böttcher et al., 2009). In addition to camalexin, a number of other pathogen-inducible indolic metabolites have been identified from leaves and roots of Arabidopsis, mainly derivatives of indole-3-carboxylic acid (ICOOH; Hagemeier et al., 2001; Bednarek et al., 2005; Iven et al., 2012). Labeling experiments demonstrated that they also originate from IAN, but the genes encoding the biosynthetic enzymes have not yet been identified (Böttcher et al., 2009). Interestingly, ICOOH is rapidly esterified to the cell wall after pathogen challenge (Tan et al., 2004; Forcat et al., 2010), plays a role as root exudate (Bednarek et al., 2005), and is also involved in β-aminobutyric acid-induced resistance (Gamir et al., 2012). In a number of other

[1] This work was supported by the Deutsche Forschungsgemeinschaft (Heisenberg Fellowship no. GL346/5 to E.G.), the Hans-Fischer-Gesellschaft, and the Technische Universität München program Chancengleichheit für Frauen in Forschung und Lehre (to M.C.).

[2] Present address: Julius Kühn-Institute, Federal Research Centre for Cultivated Plants, Königin-Luise-Straße 19, D–14195 Berlin, Germany.

* Address correspondence to egl@wzw.tum.de.

The author responsible for distribution of materials integral to the findings presented in this article in accordance with the policy described in the Instructions for Authors (www.plantphysiol.org) is: Erich Glawischnig (egl@wzw.tum.de).

[W] The online version of this article contains Web-only data.
www.plantphysiol.org/cgi/doi/10.1104/pp.114.235630

cruciferous plants, indole-3-carbaldehyde (ICHO) and ICOOH derivatives, such as the brassicanals, were identified as phytoalexins (for review see Pedras et al., 2011). In this work, using chemical complementation (i.e. the reconstitution of a biosynthetic pathway in a biosynthetic gene knockout mutant by feeding a downstream intermediate) in combination with nontargeted metabolite profiling, we comprehensively explore the spectrum of ICHO and ICOOH derivatives in leaves of Arabidopsis and show that, in response to $AgNO_3$ treatment, ICHO- and ICOOH-derived compounds accumulate in overall quantities similar to camalexin, suggesting an important role in induced chemical defense.

Aldehyde oxidases are molybdenum-containing enzymes that convert aldehydes into the corresponding carboxylic acids (Mendel and Hänsch, 2002). Arabidopsis contains four genes encoding aldehyde oxidases. ARABIDOPSIS ALDEHYDE OXIDASE3 (AAO3) catalyzes the last step in abscisic acid biosynthesis (Seo et al., 2000), and AAO4 is responsible for benzaldehyde oxidation in siliques (Ibdah et al., 2009). AAO1 and AAO2 as homodimers and heterodimers have a rather broad substrate specificity in vitro (Akaba et al., 1999; Koiwai et al., 2000), and AAO1 was recently shown to catalyze the NADH-dependent production of superoxide anions (Zarepour et al., 2012). It was proposed that aldehyde oxidases are involved in auxin biosynthesis (Seo et al., 1998), and one substrate of the AAO1 homomer is indole-3-acetaldehyde (IAAld), which is oxidized to indole-3-acetic acid (IAA) with an apparent K_m value of 39 μM (Koiwai et al., 2000). However, it is not clarified to what extent IAAld is formed in vivo. While no auxin-deficient mutant phenotype of *aao1* has yet been reported, it was recently demonstrated that the major biosynthetic pathway for IAA in plants is a two-step reaction involving Trp aminotransferases and YUCCA flavin monooxygenases but not aldehyde oxidases (Mashiguchi et al., 2011; Stepanova et al., 2011; Won et al., 2011; Kriechbaumer et al., 2012). In this article, we present evidence that the biological role of AAO1 in Arabidopsis is in the biosynthesis of defense-related indolic compounds, and we provide a model for the biosynthetic pathway of these metabolites.

RESULTS

Identification of ICHO and ICOOH Derivatives by Metabolite Profiling of Chemically Complemented *cyp79B2 cyp79B3* Mutants

We have previously shown, using 6-fluoro-IAN as a metabolic tracer, that in addition to camalexin a number of ICOOH derivatives and ICHO can be synthesized in Arabidopsis leaves from IAN (Böttcher et al., 2009). To elucidate the entire spectrum of ICHO/ICOOH derivatives accumulating in a CYP79B2/B3-dependent manner in leaf tissue, nontreated and $AgNO_3$-treated *cyp79B2 cyp79B3* leaves were fed with IAN, ICHO, and ICOOH and subjected together with nontreated and $AgNO_3$-treated mock-fed wild-type and *cyp79B2 cyp79B3* leaves to nontargeted liquid chromatography-mass spectrometry (LC-MS)-based metabolite profiling. In the first step, comparative analyses of mock-fed wild-type and *cyp79B2 cyp79B3* metabolite profiles were performed to dissect molecular features (mass-to-charge retention time pairs) associated with metabolites whose accumulation depends on CYP79B2/B3. In the next step, molecular features with significantly increased intensity in fed *cyp79B2 cyp79B3* samples in comparison with mock-fed *cyp79B2 cyp79B3* samples were identified and intersected with the set of CYP79B2/B3-dependent features. Detailed analyses and Venn diagrams are shown in Supplemental Figure S1. Based on the resulting molecular feature sets, a total of 20 metabolites was detected whose accumulation depends on CYP79B2/B3 and was reconstituted in *cyp79B2 cyp79B3* leaves by feeding of either ICHO or ICOOH (Table I). These metabolites were characterized by quadrupole-time-of-flight mass spectrometry (QTOFMS) and comprise ICOOH (1), its methyl, glucosyl, and malonylated glucosyl esters (2, 4, and 5), an ICOOH-Asp conjugate (3), and several Glc/malonyl Glc conjugates of 6-hydroxyindole-3-carboxylic acid (6-HO-ICOOH; 6–9). Besides ICHO (10), two glycosylated hydroxy-ICHO conjugates (11 and 12) were detected whose aglycones were identified after enzymatic hydrolysis as 5-hydroxyindole-3-carbaldehyde (5-HO-ICHO) and 4-hydroxyindole-3-carbaldehyde (4-HO-ICHO), respectively. In addition, ascorbigen (13), a glycosylated dihydroascorbigen (14), and six unknown metabolites (15–20), which so far could only be characterized by their elemental composition and fragmentation patterns, were found.

Reconstruction of the ICHO/ICOOH Metabolic Network

Compounds 1 to 20 were relatively quantified in nontreated and $AgNO_3$-treated mock-fed wild-type and fed *cyp79B2 cyp79B3* samples (Table II). Among the nine identified ICOOH derivatives, ICOOGlc (for β-D-glucosyl indole-3-carboxylate), 6-HO-ICOOGlc (for β-D-glucosyl 6-hydroxyindole-3-carboxylate), 6-GlcO-ICOOH (for 6-hydroxyindole-3-carboxylic acid 6-*O*-β-D-glucoside), and 6-GlcO-ICOOGlc (for β-D-glucosyl 6-hydroxyindole-3-carboxylate 6-*O*-β-D-glucoside) showed the highest absolute signal intensity after feeding of *cyp79B2 cyp79B3* with ICOOH. In addition, their high relative intensities, compared with $AgNO_3$-treated mock-fed wild-type tissue, suggest that 6-hydroxylation and *O*-glucosylation constitute the major metabolic reactions of ICOOH in leaf tissue. In contrast, conjugation with Asp or *O*-methylation, the latter occurring exclusively in $AgNO_3$-treated leaf tissue, represent minor metabolic transformations of ICOOH.

After chemical complementation of *cyp79B2 cyp79B3* with ICHO, the compounds 5-GlcO-ICHO (for 5-hydroxyindole-3-carbaldehyde 5-*O*-β-D-glucoside),

Table I. *Analytical data of identified ICHO/ICOOH derivatives*

Δm, Mass error.

No.	Compound	ID[a]	Elemental Composition	Retention Time	Quantifier Ion			Observed Fragment Ions upon CID[b] Precursor Ion Marked in Boldface
					Type	Measured *m/z*	Δm	
				s			*ppm*	
1	ICOOH	a	$C_9H_7NO_2$	284	$[M-H]^-$	160.0400	2.7	**160**, 116
2	ICOOMe	a	$C_{10}H_9NO_2$	400	$[M-H]^-$	174.0556	2.7	**174**, 159, 144, 142, 131, 115
3	*N*-ICO-Asp	d	$C_{13}H_{12}N_2O_5$	231	$[M-H]^-$	275.0667	2.4	**275**, 160, 132, 115
4	ICOOGlc	b, c, d	$C_{15}H_{17}NO_7$	227	$[M-H]^-$	322.0932	−0.8	**322**, 262, 232, 202, 179, 160
5	ICOO(MalonylGlc)	c, d	$C_{18}H_{19}NO_{10}$	275	$[M-H-CO_2]^-$	364.1033	1.5	**364**, 304, 244, 232, 214, 202, 160, 116, 113, 101
6	6-HO-ICOOGlc	b, c, d	$C_{15}H_{17}NO_8$	117	$[M-H]^-$	338.0880	0.6	**338**, 278, 248, 218, 179, 176, 161, 158, 143, 132, 119, 113, 101
7	6-GlcO-ICOOH	b, c, d	$C_{15}H_{17}NO_8$	101	$[M-H]^-$	338.0875	1.8	**338**, 218, 176, 175, 132
8	6-(MalonylGlcO)-ICOOH	c, d	$C_{18}H_{19}NO_{11}$	194	$[M-H-CO_2]^-$	380.0982	1.3	**380**, 176, 175, 132
9	6-GlcO-ICOOGlc	b, c, d	$C_{21}H_{27}NO_{13}$	62	$[M-H]^-$	500.1402	1.4	**500**, 440, 410, 380, 338, 278, 248, 218, 176, 132, 113, 101
10	ICHO	a	C_9H_7NO	288	$[M-H]^-$	144.0452	2.0	**144**, 142, 126, 116, 115
11	5-GlcO-ICHO	b, c, d	$C_{15}H_{17}NO_7$	112	$[M-H]^-$	322.0926	2.1	**322**, 232, 214, 202, 186, 174, 159, 131
12	4-GlcO-ICHO	b, d	$C_{15}H_{17}NO_8$	155	$[M-H]^-$	322.0932	−2.6	**322**, 202, 160, 159, 132, 131
13	Ascorbigen	a	$C_{15}H_{15}NO_6$	252	$[M-H]^-$	304.0815	3.7	**304**, 244, 216, 204, 200, 188, 186, 175, 157, 139, 116, 115
14	Dihydroascorbigen hexoside	d	$C_{21}H_{27}NO_{11}$	207	$[M-H]^-$	468.1490	4.5	**468**, 288, 246, 226, 218, 216, 210, 204, 188, 179, 172, 158, 116
U15	Hexoside of $C_9H_7NO_3$	d	$C_{15}H_{17}NO_8$	149	$[M-H]^-$	338.0869	3.6	**338**, 176, 175
U16	Hexoside of $C_9H_7NO_3$	d	$C_{15}H_{17}NO_8$	176	$[M-H]^-$	338.0881	0.1	**338**, 176, 132
U17	Hexoside of $C_9H_7NO_3$	d	$C_{15}H_{17}NO_8$	213	$[M-H]^-$	338.0872	2.7	**338**, 218, 176, 175
U18	Unknown	–	$C_{12}H_{12}N_2O_4$	164	$[M-H]^-$	247.0717	3.0	**247**, 160, 116
U19	Unknown	–	$C_{12}H_{12}N_2O_4$	181	$[M-H]^-$	247.0716	3.4	**247**, 160, 132
U20	Unknown	–	$C_{12}H_{12}N_2O_3$	166	$[M-H]^-$	231.0764	5.0	**231**, 144

[a]Identification: a, identified using an authenticated standard; b, compound isolated by preparative HPLC from $AgNO_3$-treated Col-0 leaves and hydrolyzed using a β-glucosidase, with aglycone afterward identified using an authenticated standard; c, compound with identical chromatographic and mass spectral properties formed after feeding the respective aglycone to *cyp79B2 cyp79B3* leaves; d, interpretation of mass spectral data. [b]For completely interpreted CID mass spectra, see Supplemental Table S1.

ICOOGlc, 6-HO-ICOOGlc, 6-GlcO-ICOOH, and 6-GlcO-ICOOGlc appear as major derivatives, indicating that ICHO is either metabolized by 5-hydroxylation and *O*-glucosylation or oxidized to ICOOH and metabolized by 6-hydroxylation and *O*-glucosylation. Interestingly, exogenously supplied ICHO was also incorporated into ascorbigen and a glycosylated dihydroascorbigen, suggesting that ICHO is reduced to a minor extent to indole-3-carbinol, which is subsequently trapped by ascorbic acid. A further minor metabolic route was 4-hydroxylation and *O*-glucosylation to give 4-GlcO-ICHO (for 4-hydroxyindole-3-carbaldehyde 4-*O*-β-D-glucoside).

It should be noted that all identified ICHO/ICOOH derivatives 1 to 20 were below the detection limit in nontreated/$AgNO_3$-treated mock-fed *cyp79B2 cyp79B3* and could be reconstituted by feeding of *cyp79B2 cyp79B3* with IAN. In contrast, camalexin was exclusively restored in *cyp79B2 cyp79B3* by feeding with IAN but not ICHO or ICOOH.

Based on the chemical complementation studies, Figure 1 presents a putative biosynthetic scheme of ICHO/ICOOH derivatives.

Quantification of ICHO and ICOOH Derivative Pools

In order to quantify ICHO/ICOOH derivative pool sizes, methanolic extracts prepared from nontreated and $AgNO_3$-treated wild-type leaves were digested with a β-glucosidase, and the released indolic aglycones were analyzed by LC-MS (Fig. 2). In contrast to camalexin, which was near or below the detection limit, low constitutive levels of 4-HO-ICHO, 5-HO-ICHO, ICOOH, and 6-HO-ICOOH were already detectable in nontreated wild-type leaves. Following $AgNO_3$ treatment, pool sizes of all ICHO/ICOOH derivatives were found to be increased. Thereby, ICHO, ICOOH, and methyl indole-3-carboxylate (ICOOMe) showed the highest relative change in comparison with their constitutive accumulation levels. Notably, the total level of all ICHO/ICOOH derivatives

Table II. *Relative quantification of identified ICHO/ICOOH derivatives and camalexin in nontreated/$AgNO_3$-treated wild-type and cyp79B2 cyp79B3 leaves with or without chemical complementation*

Compounds 1 to 20 were quantified by UPLC/ESI(−)-QTOFMS using extracted ion chromatograms of respective quantifier ions (Table I). Camalexin was quantified by UPLC/ESI(+)-QTOFMS via its protonated molecular ion. Values shown are median peak areas per fresh weight (counts $mg^{-1} \times 10^3$) ± SD ($n = 5$). w/o, Without; n.d., not detected.

No.	Compound	Genotype/Treatment/Chemical Complementation									
		Col-0 w/o Mock	Col-0 $AgNO_3$ Mock	*cyp79B2/B3* w/o Mock	*cyp79B2/B3* $AgNO_3$ Mock	*cyp79B2/B3* w/o IAN	*cyp79B2/B3* $AgNO_3$ IAN	*cyp79B2/B3* w/o ICHO	*cyp79B2/B3* $AgNO_3$ ICHO	*cyp79B2/B3* w/o ICOOH	*cyp79B2/B3* $AgNO_3$ ICOOH
1	ICOOH	n.d.	0.12 ± 0.03	n.d.	n.d.	0.03 ± 0.03	0.38 ± 0.04	0.04 ± 0.05	0.24 ± 0.04	0.83 ± 0.30	1.21 ± 0.17
2	ICOOMe	n.d.	0.63 ± 0.10	n.d.	n.d.	n.d.	0.71 ± 0.11	n.d.	0.31 ± 0.15	n.d.	0.33 ± 0.30
3	*N*-ICO-Asp	n.d.	0.05 ± 0.03	n.d.	n.d.	1.79 ± 0.24	0.29 ± 0.04	0.18 ± 0.05	n.d.	0.05 ± 0.03	0.05 ± 0.04
4	ICOOGlc	0.37 ± 0.06	6.13 ± 1.14	n.d.	n.d.	31.2 ± 4.04	10.6 ± 1.15	43.6 ± 4.18	16.6 ± 4.48	53.6 ± 7.73	43.3 ± 4.54
5	ICOO(MalonylGlc)	n.d.	0.07 ± 0.02	n.d.	n.d.	0.38 ± 0.08	0.15 ± 0.04	0.45 ± 0.06	0.12 ± 0.02	1.78 ± 0.91	1.41 ± 0.26
6	6-HO-ICOOGlc	n.d.	1.05 ± 0.15	n.d.	n.d.	7.34 ± 1.10	2.48 ± 0.22	22.2 ± 5.66	4.51 ± 1.38	18.4 ± 1.62	19.9 ± 4.80
7	6-GlcO-ICOOH	1.17 ± 0.12	5.25 ± 1.07	n.d.	n.d.	20.3 ± 2.35	9.45 ± 0.98	30.3 ± 3.40	12.9 ± 2.87	23.1 ± 2.09	20.1 ± 3.19
8	6-(MalonylGlcO)-ICOOH	n.d.	0.05 ± 0.03	n.d.	n.d.	0.21 ± 0.04	0.10 ± 0.03	0.25 ± 0.03	0.05 ± 0.01	0.33 ± 0.04	0.29 ± 0.05
9	6-GlcO-ICOOGlc	0.37 ± 0.02	0.60 ± 0.16	n.d.	n.d.	3.40 ± 0.47	1.01 ± 0.18	4.81 ± 0.52	1.16 ± 0.31	4.15 ± 0.38	3.51 ± 0.58
10	ICHO	n.d.	0.86 ± 0.24	n.d.	n.d.	0.08 ± 0.13	2.44 ± 0.47	5.44 ± 1.63	17.5 ± 3.34	n.d.	n.d.
11	5-GlcO-ICHO	1.14 ± 0.05	1.90 ± 0.29	n.d.	n.d.	8.47 ± 2.44	3.07 ± 0.43	24.8 ± 2.81	10.1 ± 2.41	n.d.	n.d.
12	4-GlcO-ICHO	0.20 ± 0.02	0.40 ± 0.08	n.d.	n.d.	0.11 ± 0.03	0.04 ± 0.03	0.33 ± 0.03	0.09 ± 0.01	n.d.	n.d.
13	Ascorbigen	0.31 ± 0.08	0.48 ± 0.30	n.d.	n.d.	0.14 ± 0.04	0.24 ± 0.08	0.41 ± 0.08	0.60 ± 0.12	n.d.	n.d.
14	Dihydroascorbigen hexoside	0.81 ± 0.04	1.83 ± 0.13	n.d.	n.d.	0.27 ± 0.10	0.11 ± 0.03	1.12 ± 0.24	0.96 ± 0.55	n.d.	n.d.
U15	Hexoside of $C_9H_7NO_3$	0.07 ± 0.01	0.14 ± 0.04	n.d.	n.d.	0.32 ± 0.12	0.06 ± 0.01	0.71 ± 0.12	0.17 ± 0.04	n.d.	n.d.
U16	Hexoside of $C_9H_7NO_3$	n.d.	0.09 ± 0.01	n.d.	n.d.	0.32 ± 0.02	0.17 ± 0.01	0.58 ± 0.12	0.25 ± 0.05	0.50 ± 0.07	0.61 ± 0.13
U17	Hexoside of $C_9H_7NO_3$	0.25 ± 0.04	0.36 ± 0.13	n.d.	n.d.	0.84 ± 0.24	0.13 ± 0.03	2.72 ± 0.55	0.30 ± 0.09	n.d.	n.d.
U18	–	n.d.	0.07 ± 0.02	n.d.	n.d.	0.44 ± 0.11	0.06 ± 0.01	0.73 ± 0.25	0.13 ± 0.06	n.d.	n.d.
U19	–	0.37 ± 0.02	0.55 ± 0.19	n.d.	n.d.	0.72 ± 0.14	0.07 ± 0.04	1.87 ± 0.29	0.18 ± 0.05	n.d.	n.d.
U20	–	n.d.	0.11 ± 0.02	n.d.	n.d.	0.38 ± 0.09	0.13 ± 0.02	0.77 ± 0.33	0.68 ± 0.31	n.d.	n.d.
	Camalexin	n.d.	30.3 ± 11.2	n.d.	n.d.	16.7 ± 5.85	14.9 ± 1.00	n.d.	n.d.	n.d.	n.d.

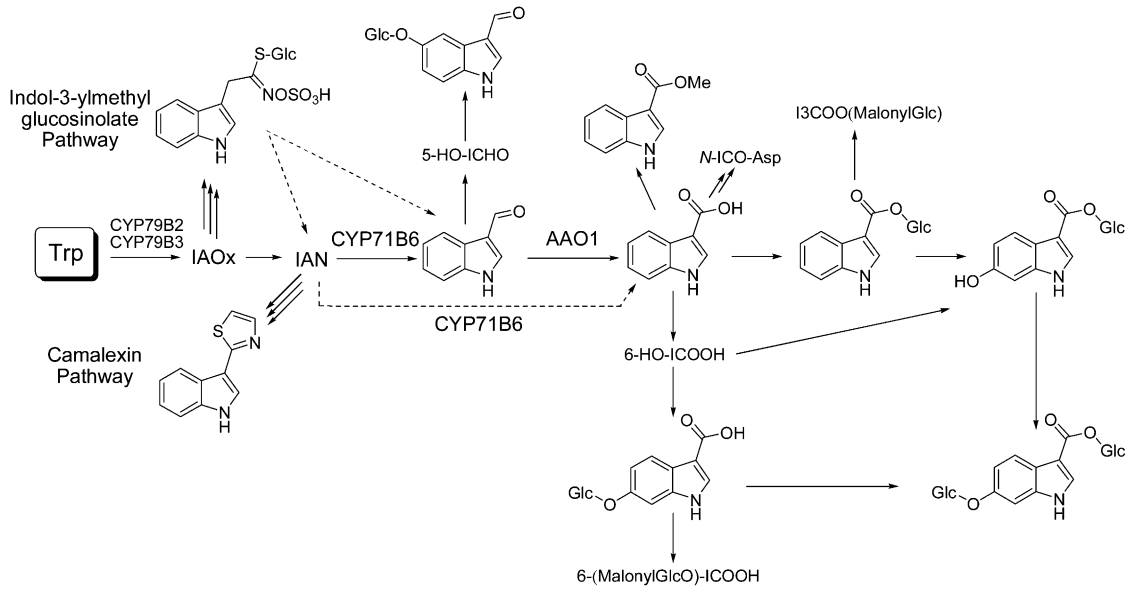

Figure 1. Putative biosynthetic pathways of ICHO/ICOOH derivatives based on the chemical complementation of the *cyp79B2 cyp79B3* mutant and phenotypic analysis of the *aao1* and *cyp71B6* knockout lines. The enzymatic functions of CYP71B6 and AAO1 are indicated.

was in the range of the camalexin level 24 h after $AgNO_3$ treatment.

AAO1 Is Transcriptionally Coexpressed with Camalexin Biosynthetic Genes

In addition to the in vitro substrate IAAld, heterologously expressed Arabidopsis AAO1 has been shown previously to convert ICHO into ICOOH with an apparent K_m value of 4.4 μM (Koiwai et al., 2000). To evaluate whether AAO1 could be involved in the biosynthesis of pathogen-inducible derivatives of ICOOH, we performed a transcriptome coexpression analysis based on microarray experiments from the AtGenExpress pathogen compendium using the Expression Angler platform (Toufighi et al., 2005) with *AAO1* as the query gene. Strikingly, significant coexpression with the camalexin biosynthetic genes *CYP71A13* and *CYP71B15*, the transcription factor *ANAC042*, which is involved in the regulation of camalexin biosynthesis (Saga et al., 2012), and *CYP71B6* (see below) was observed (Table III). A comprehensive coexpression analysis of *AAO1* and *CYP71B6* for different subsets of microarray and RNA sequencing data was performed applying the ATTED-II platform (Obayashi et al., 2014; Supplemental Table S2), confirming the coexpression of *AAO1* and *CYP71B6* with camalexin-related genes and with each other. This suggested that *AAO1* and *CYP71B6* might function in induced chemical defense.

Enzymatic Activity of CYP71B6

Previously, using *Escherichia coli* spheroblasts, in vitro turnover of IAN was demonstrated in the Halkier laboratory for CYP71B6 and ICHO was identified as a product (Nafisi, 2007). To prove this result using an independent heterologous expression system and to characterize CYP71B6 in more detail, it was expressed in the yeast (*Saccharomyces cerevisiae*) strain WAT11. NADPH-dependent IAN turnover to ICHO and to a lesser extent (approximately 17%) also to ICOOH was detected (Fig. 3, A and B). Similar to the turnover of Cys(IAN) by CYP71B15 (Böttcher et al., 2009), this reaction was accompanied by a stoichiometric NADPH-dependent release of cyanide, which was quantified after derivatization with 2,3-naphthalenedialdehyde and taurine (Fig. 3, A and C). When ICHO was applied as substrate, no ICOOH formation was observed (data not shown).

The kinetic properties of CYP71B6 were determined (Supplemental Fig. S2): apparent $k_{cat} = (92 \pm 3)\ 10^{-3}\ s^{-1}$; apparent K_m (IAN) = 0.23 ± 0.02 μM. Strikingly, the K_m value for its substrate is 1 to 2 orders of magnitude lower compared with other CYP71 enzymes (for CYP71C1, CYP71C2, CYP71C3, and CYP71C4, see Glawischnig et al., 1999; for CYP71B15, see Schuhegger et al., 2006). In conclusion, given a calculated catalytic efficiency of approximately 0.4 $\mu M^{-1}\ s^{-1}$, CYP71B6 is effectively metabolizing IAN.

Establishment of *CYP71B6* and *AAO1* Overexpression Lines

AAO1 and *CYP71B6* are low and moderately expressed in nontreated rosette leaves, respectively (http://bbc.botany.utoronto.ca/efp), whereas transcript levels of both genes are highly induced 18 h after $AgNO_3$ treatment (*AAO1* more than 1,000-fold, *CYP71B6*

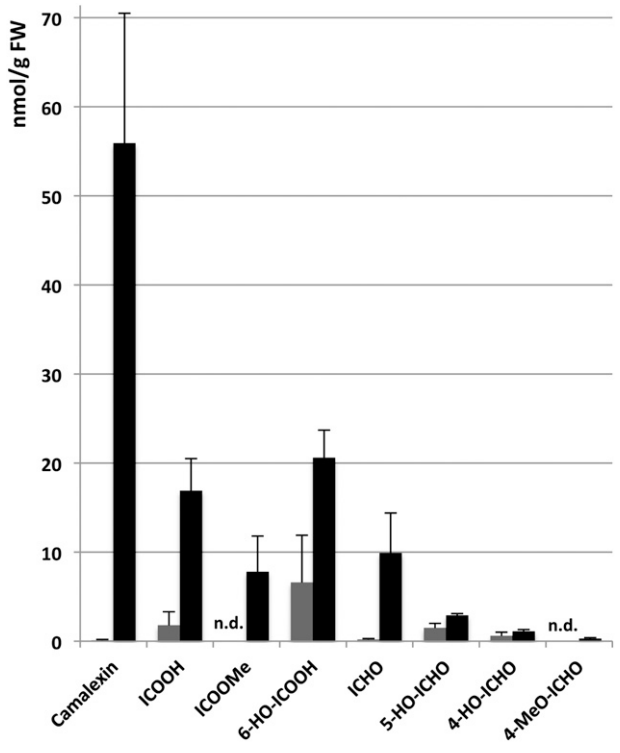

Figure 2. Absolute quantification of ICHO/ICOOH derivative pool sizes and camalexin in rosette leaves of nontreated (gray bars) and $AgNO_3$-treated (24 h after treatment; black bars) Col-0 plants. Rosette leaves of 10 nontreated/treated plants, cultivated in two independent experiments, were individually pooled and extracted. After treatment with a β-glucosidase, ICHO/ICOOH derivatives were quantified by UPLC/ESI(+)-QTOFMS. 5-HO-ICOOH and 6-HO-ICHO were below the detection limit (less than 0.2 and less than 0.1 nmol g^{-1} fresh weight [FW], respectively). Error bars indicate SD (n = 10); n.d., not detected.

approximately 282-fold; Supplemental Fig. S3). To investigate the effect of strong constitutive expression of these genes, *CYP71B6* and *AAO1* were cloned into pCAMBIA330035Su and corresponding overexpression lines were generated. Constitutive expression of the transgenes was evaluated by quantitative reverse transcription-PCR. Three CYP71B6 overexpression lines with more than 100-fold expression in relation to the wild type (approximately 194-fold [line 2], 178-fold [line 3], and 132-fold [line 4]) were identified, and lines 2 and 4 were selected for detailed analysis.

One AAO1 overexpression line with an approximately 373-fold expression level compared with the wild type was identified. To address whether the *AAO1* genotype affects the in vitro turnover of ICHO to ICOOH, total protein extracts from rosette leaves of Columbia-0 (Col-0), the *aao1* transfer DNA (T-DNA) insertion mutant, and *35S:AAO1* were prepared and analyzed for aldehyde oxidase activity using ICHO as substrate. ICHO oxidase activity was reduced significantly in *aao1* and enhanced in *35S:AAO1* (Supplemental Fig. S4) in comparison with the wild type. This showed that AAO1 contributes significantly to ICOOH formation in vitro.

Metabolite Profiling of Knockout and Overexpression Lines

In order to elucidate the role of CYP71B6 and AAO1 in the biosynthesis of soluble ICHO/ICOOH derivatives, their accumulation levels in rosette leaves of the established *CYP71B6* and *AAO1* knockout and overexpression lines were determined relative to the wild type (Supplemental Table S3). In nontreated leaves, the accumulation levels of ICHO/ICOOH derivatives were not dependent on the *CYP71B6* genotype (Fig. 4; Supplemental Table S4). In contrast, 24 h after the induction of ICHO/ICOOH biosynthesis by $AgNO_3$ treatment, the level of ICOOGlc was consistently reduced in *cyp71B6-1* and *cyp71B6-2* to 82% (P = 2.0E-03) and 79% (P = 2.9E-03) of the wild-type level (Supplemental Table S5). A similar trend was observed for the other ICOOH derivatives, ICOOMe, 6-HO-ICOOGlc, 6-GlcO-ICOOH, and 6-GlcO-ICOOGlc, although without statistical significance. This suggests that CYP71B6 functions in ICOOH derivative biosynthesis in vivo (Fig. 1) at least after $AgNO_3$ treatment and that functionally homologous enzymes exist. As observed for nontreated leaves, the accumulation levels of ICHO/ICOOH derivatives remained unchanged upon the overexpression of *CYP71B6*. In all lines, the level of the precursor IAN was below the detection limit.

In nontreated *aao1* mutant leaves, the level of 5-GlcO-ICHO was increased significantly to 170% (P = 5.4E-08) of the wild-type level, whereas *AAO1* overexpression resulted in a reduction of 5-GlcO-ICHO to 53% (P = 4.1E-04) of the wild-type level (Fig. 4). For the levels of ICOOGlc, 6-GlcO-ICOOH, and 6-GlcO-ICOOGlc, the opposite trend to that observed for 5-GlcO-ICHO became apparent in *AAO1* knockout and overexpression lines compared with the wild type, albeit with a lower effect size and hence without statistical significance. However, following direct pairwise comparison of *AAO1* knockout and overexpression lines, the difference in the accumulation levels of 6-GlcO-ICOOH and 6-GlcO-ICOOGlc was statistically significant ($P < 2.0E-03$). After $AgNO_3$ treatment, the level of 5-GlcO-ICHO was again increased significantly in *aao1* to 139% (P = 3.1E-09) of the wild-type level (Fig. 4). In contrast, *AAO1* overexpression correlated with significantly decreased levels of both ICHO and 5-GlcO-ICHO, which accumulated to 64% (P = 7.7E-04) and 60% (P = 3.6E-09) of the wild-type level.

The observed chemotypes of *AAO1* knockout and overexpression lines suggest that AAO1 is involved in the oxidation of ICHO to ICOOH in both nontreated and $AgNO_3$-treated leaves (Fig. 1).

To test whether *CYP71B6* and *AAO1* knockout and overexpression impact the level of cell wall-associated ICOOH, cell wall preparations of nontreated and $AgNO_3$-treated rosette leaves of wild-type and mutant

Table III. *Genes transcriptionally coexpressed with AAO1*

Expression Angler and the AtGenExpress pathogen compendium were used. Most significant hits are shown. Proteins related to phytoalexin induction are printed in bold.

Gene	r^2	Protein	Biological Function	Reference
At1g33030	0.932	*O*-Methyltransferase	Unknown	
At4g38540	0.929	FAD/NAD(P)-binding oxidoreductase	Unknown	
At2g30770	0.926	**CYP71A13**	Camalexin biosynthesis	Nafisi et al. (2007)
At4g19370	0.924	DUF1218	Unknown	
At2g24180	0.924	**CYP71B6**	Biosynthesis of ICHO/ICOOH derivatives	This study
At3g48890	0.922	ATMAPR3_ATMP2_MAPR3_MSBP2	Unknown	
At3g26830	0.921	**CYP71B15_PAD3**	Camalexin biosynthesis	Zhou et al. (1999); Schuhegger et al. (2006); Böttcher et al. (2009)
At3g48850	0.912	PHT3;2	Unknown	
At2g43000	0.906	**ANAC042**	Camalexin and longevity regulation	Saga et al. (2012); Wu et al. (2012)

plants were hydrolyzed, and the ICOOH released was quantified (Supplemental Fig. S5). As observed for the soluble ICOOH fraction of wild-type leaves, the level of cell wall-bound ICOOH increased strongly 24 h after $AgNO_3$ (more than 10-fold) in comparison with nontreated leaves. Neither *CYP71B6* nor *AAO1* knockout or overexpression resulted in a pronounced chemotype for cell wall-bound ICOOH in $AgNO_3$-treated or nontreated leaves, reflecting the observations made for the soluble ICOOH fraction.

DISCUSSION

Proposed Biosynthetic Pathways of ICHO-Derived Secondary Metabolites

In a number of Arabidopsis metabolite profiling studies including different organs, derivatives of ICHO and ICOOH were detected and their concentrations were shown to increase upon pathogen infection (Hagemeier et al., 2001; Bednarek et al., 2005; Böttcher et al., 2009). Nevertheless, while the biosynthetic pathway and the biological function of the characteristic Arabidopsis phytoalexin camalexin are well understood, these metabolites have been largely neglected. This is probably due to the formation of a rather complex blend of derivatives instead of one striking major metabolite. In a previous study (Böttcher et al., 2009), we have shown that they are synthesized via CYP79B2- and CYP79B3-dependent IAOx formation and, according to incorporation experiments, via IAN. Here, we have similarly applied ICHO and ICOOH to *cyp79B2 cyp79B3* leaves and subsequently used LC-MS-based metabolite profiling to explore the composition of ICHO and ICOOH derivatives. As major compounds, Glc conjugates of 5-HO-ICHO, ICOOH, and 6-HO-ICOOH were identified. The pattern of metabolites in chemically complemented *cyp79B2 cyp79B3* leaves was consistent with a biosynthetic pathway via IAN, ICHO, and ICOOH for ICOOH derivatives. As observed for camalexin (Böttcher et al., 2009), hydroxylated derivatives of ICHO and ICOOH were found to accumulate, notably with a distinct substitution pattern. While 5-HO-ICHO and 6-HO-ICOOH were identified as major aglycones after β-glucosidase treatment, the levels of 6-hydroxyindole-3-carbaldehyde (6-HO-ICHO) and 5-hydroxyindole-3-carboxylic acid (5-HO-ICOOH) were below the detection limit. This indicates that either ICHO and ICOOH are specifically hydroxylated in vivo in the 5- and 6-positions, respectively, or alternatively, intermediary 6-OH-ICHO is selectively oxidized to 6-HO-ICOOH.

Chemical complementation of *cyp79B2 cyp79B3* with ICHO revealed that ICHO is incorporated to a minor extent into 4-GlcO-ICHO, ascorbigen, and dihydroascorbigen hexoside. Since ascorbigen is a well-known breakdown product of IMG (Agerbirk et al., 2009) and 4-hydroxylation of the indole ring represents a characteristic modification reaction of IMG (Pfalz et al., 2009), it can be assumed that the native accumulation of these metabolites in nontreated and $AgNO_3$-treated wild-type leaves is probably associated with indole glucosinolate metabolism. The artificial incorporation of exogenously supplied ICHO into these putative glucosinolate catabolites might be caused by high concentrations of ICHO in leaf tissue during the feeding experiment.

In turnip (*Brassica rapa*) roots, ICHO and ICOOH were identified as primary in vivo breakdown products of isotopically labeled IMG (Pedras et al., 2002). For Arabidopsis, it is currently unclear whether IMG catabolism additionally contributes, via oxidation of the primary formed indole-3-carbinol, to the accumulation of ICHO and ICOOH derivatives. However, the action of this pathway could explain the basal levels of ICHO and ICOOH derivatives in nontreated leaves.

Recently, it was speculated that camalexin could be synthesized via an alternative pathway involving GH3.5-catalyzed conjugation of ICOOH with Cys (Wang et al., 2012). We have not detected any camalexin in *cyp79B2 cyp79B3* plants incubated with ICHO or ICOOH. This indicates that this reaction is not relevant in vivo and that, rather, *GH3.5* overexpression results in stress reactions, including the observed induction of established biosynthetic genes.

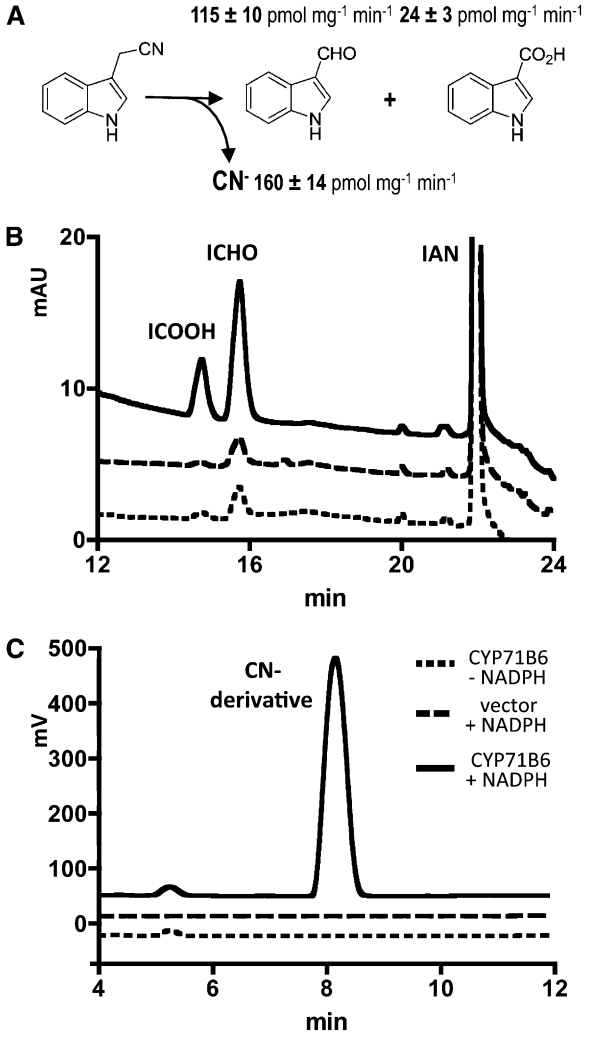

Figure 3. CYP71B6 enzymatic activity. CYP71B6 was expressed in yeast, and enzymatic turnover of IAN (5 nmol, 200 μM) to ICHO, ICOOH, and cyanide was detected. A, Product spectrum (n = 9). Cyanide (CN^-) is a stoichiometric by-product. B and C, Representative HPLC chromatograms. B, Detection of indolic compounds at 278 nm. mAU, Milliabsorbance units. C, Detection of a cyanide derivative. Fluorescence, 418 nm (excitation)/460 nm (emission).

Contribution of AAO1 and CYP71B6 to the Biosynthesis of ICOOH-Derived Secondary Metabolites in Arabidopsis

CYP71B6 and AAO1 catalyze the formation of ICHO/ICOOH and ICOOH, respectively, in vitro and are transcriptionally coexpressed with known enzymes of camalexin biosynthesis. Therefore, we have analyzed the profile of IAOx-derived secondary metabolites in knockout and overexpression plants of *CYP71B6* and *AAO1*. Most strikingly, *aao1* T-DNA insertion mutants accumulate 5-GlcO-ICHO, while this derivative of the intermediate ICHO is significantly reduced in *AAO1* overexpressors. This is in accordance with the frequent observation (Geu-Flores et al., 2009) that the effects on the level of a substrate (derivative) are highly significant, in this case $P < 0.001$ (Student's t test), while the effect on the product spectrum is subtle when partially redundant enzymes are expressed. Candidates for functioning redundantly to AAO1 are Arabidopsis AAO2 and CYP71B6, for which we have shown in vitro that it synthesizes ICOOH. The level of 4-GlcO-ICHO was not affected by *AAO1* knockout or overexpression either in nontreated or $AgNO_3$-treated leaves, supporting the hypothesis that this ICHO derivative has a different biosynthetic origin than 5-GlcO-ICHO.

We observed reduced levels of ICOOGlc in $AgNO_3$-induced *cyp71B6* knockout mutants in relation to wild-type plants, while for untreated plants no difference was observed. CYP71B6 is a member of a large gene family, and we speculate that other cytochrome P450 enzymes, such as CYP71A12/A13 (Klein et al., 2013), have overlapping biochemical functions and expression patterns, explaining the rather mild metabolic phenotype of *cyp71b6* knockout mutants, despite the high catalytic efficiency of CYP71B6 for its substrate IAN (approximately 0.4 μM^{-1} s^{-1}) in vitro. To evaluate the function of ICHO-derived metabolites in pathogen resistance in vivo, it will be necessary to analyze multiple mutants or to engineer the whole pathway for overexpression. CYP71B6 overexpression alone did not result in a further enhancement of ICOOH derivative levels, indicating that this biosynthetic step is not rate limiting in wild-type plants.

In vitro, IAN turnover by CYP71B6 resulted in ICOOH as a product in addition to ICHO, while no direct turnover of ICHO was detected. We speculate that an α-hydroxynitril is formed as an unstable intermediate, which decomposes to ICHO and hydrogen cyanide. Possibly, this intermediate can be oxidized a second time by CYP71B6, and subsequently, this α,α-dihydroxynitrile decomposes to ICOOH and hydrogen cyanide. Dual hydroxylation of the same position has been shown, for example, for CYP79 enzymes (Sibbesen et al., 1994). In the CYP71B6-catalyzed IAN turnover, stoichiometric amounts of cyanide were released in vitro. Previously, we searched for the established cyanide metabolites β-cyanoalanine and γ-glutamyl-β-cyanoalanine in extracts of $AgNO_3$-treated leaves, which were not detectable (Böttcher et al., 2009). Possibly, cyanide released by CYP71B6 and other enzymes catalyzing the same reaction is recycled efficiently into central metabolism. As both cytochrome P450s as well as AAO1 (Zarepour et al., 2012) are inhibited by cyanide, rapid removal of this by-product is necessary to prevent shutdown of the biosynthetic pathway. Recently, it was demonstrated that low amounts of cyanide (approximately 0.08 nmol g^{-1} fresh weight) accumulate in response to *Botrytis cinerea* infection (García et al., 2013). We propose that, in addition to ethylene biosynthesis, IAN (this study) and Cys(IAN) (Böttcher et al., 2009) turnover might be another source of cyanide. As in response to *B. cinerea* infection camalexin alone is synthesized in concentrations

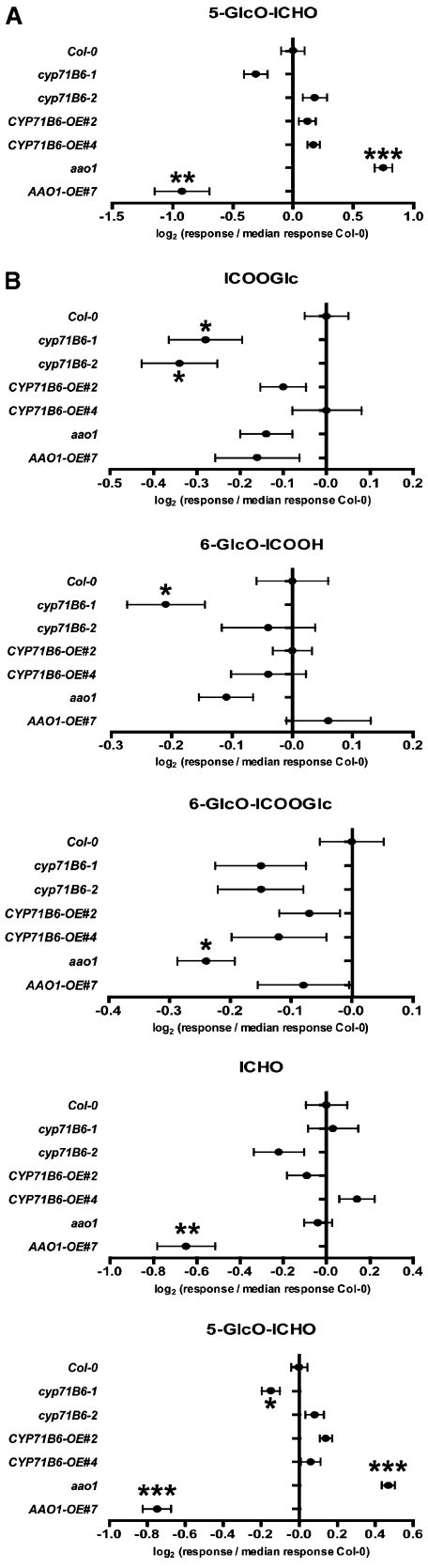

Figure 4. Relative quantification of ICHO/ICOOH derivatives in rosette leaves of wild-type (Col-0) and mutant plants nontreated (A) or 24 h after spraying 5 mM $AgNO_3$ (B). Metabolites for which significant differences were observed are shown. The full data set is presented in Supplemental Tables S4 and S5. Error bars indicate SE (n = 16–18). Significance analysis of differences between the wild type and mutant was performed by Student's t test (two-tailed, unequal variances; *$P \leq$ 10E-02, **$P \leq$ 10E-03, ***$P \leq$ 10E-04).

approximately 1,000-fold higher (Denby et al., 2004) with respect to cyanide (García et al., 2013), also here, stoichiometrically synthesized cyanide was efficiently detoxified. In mutants partially defective in cyanide detoxification, genes involved in defense are transcriptionally up-regulated (García et al., 2013). This indicates that the remaining cyanide might contribute to a positive feedback loop.

Evolution of Phytoalexin Biosynthesis in the Brassicaceae

In response to $AgNO_3$, we detected overall levels of ICHO-derived metabolites similar to camalexin, suggesting a major biological function. Recently, the phylogenetic distribution of indolic phytoalexins in cruciferous plants was studied (Bednarek et al., 2011). It was demonstrated that ICOOH derivatives are also present in the more distantly related *Cardamine hirsuta* in addition to camalexin-synthesizing members of the Brassicaceae. Therefore, we postulate that the formation of ICHO from IAN by enzymes such as CYP71B6 is a more ancient reaction, from which possibly the activation of IAN and subsequent conjugation with glutathione, yielding glutathione-IAN, has evolved in the common ancestor of *Capsella* species and Arabidopsis.

ICHO or ICOOH has been detected in species outside the Brassicaceae, including pea (*Pisum sativum*) seedlings, where ICHO was identified as an inhibitor of lateral bud growth (Nakajima et al., 2002), and the gymnosperm *Pinus sylvestris* (Sandberg et al., 1984). Here, approximately 14 pmol g^{-1} fresh weight ICOOH was found in needles, which is more than 2 orders of magnitudes less than in unchallenged Arabidopsis leaves (Fig. 2). ICOOH has been attributed to the degradation of IAA. This auxin degradation pathway is not yet understood in detail. We speculate that ICHO and ICOOH or derivatives thereof can be frequently observed in plants in very small amounts as IAA degradation products. In the Brassicaceae, this route probably contributes to only a very minor extent to the biosynthesis of these compounds.

Aldehyde oxidases are widely distributed in genomes of plants, even in species for which no ICOOH derivatives are described. We hypothesize that, during the evolution of ICOOH biosynthesis in a common ancestor of Arabidopsis and *Cardamine* spp., an aldehyde oxidase with broad substrate specificity was recruited. Then, a pathogen-inducible expression pattern and ICHO as a preferred substrate evolved.

MATERIALS AND METHODS

Chemicals

5-HO-ICHO and 6-HO-ICHO were prepared from 5- and 6-hydroxyindole (Sigma-Aldrich) by Vilsmeier-Haack reaction using dimethylformamide and phosphoryl chloride. Ascorbigen A was prepared from indole-3-carbinole (Sigma-Aldrich) and ascorbic acid (Kiss and Neukomm, 1966). 4-HO-ICHO was purchased from Apollo Scientific (www.apolloscientific.co.uk), 4-methoxyindole-3-carbaldehyde from Chem-Impex International (www.chemimpex.com), 5-HO-ICOOH from Debye Scientific (www.debyesci.com), 6-HO-ICOOH from Sphinx Scientific Laboratory (www.sphinxscientificlab.com), and ICOOMe from OlChemIm (www.olchemim.cz). ICHO, 5-methoxyindole-3-carbaldehyde (5-MeO-ICHO), and ICOOH were obtained from Sigma-Aldrich.

Plant Growth

For feeding and metabolite profiling experiments, Arabidopsis (*Arabidopsis thaliana*) wild-type and mutant lines were sown on a soil:vermiculite mixture (3:2), cold stratified for 3 d at 4°C, and grown in parallel in a growth cabinet with 8 h of light (approximately 150 μE m^{-2} s^{-1})/22°C and 16 h of dark/21°C at 60% relative humidity. After 2 weeks, plantlets were transplanted into 8-cm pots, randomly arrayed in four-by-six grids in trays, and grown for an additional 4 weeks to developmental stage 3.5 (Boyes et al., 2001). For transformation and for RNA and protein isolation, plants were grown in a growth chamber with a 12/12-h photoperiod at 80 to 100 μmol m^{-2} s^{-1}, 21°C, and 40% relative humidity.

In Vivo Feeding Experiments

Six-week-old Col-0 and *cyp79B2 cyp79B3* (Zhao et al., 2002) plants were sprayed with 5 mM $AgNO_3$ or water 1 h after the beginning of the photoperiod. After 2 h, four uniform rosette leaves per plant were excised at the petiole and immersed in PCR tubes containing 200 μL of the corresponding feeding solution (200 μM indole derivative in ethanol:water, 2:98 [v/v] or ethanol: water, 2:98 [v/v] as a control). After incubation for 24 h, rosette leaves were pooled, frozen, and homogenized in liquid nitrogen. Ground leaf material (50 ± 3 mg) was extracted twice with 200 μL of methanol:water, 80:20 (v/v) as described previously (Böttcher et al., 2009). The combined extracts were evaporated to dryness in a vacuum centrifuge at 30°C. The remaining residue was reconstituted in 100 μL of methanol:water, 30:70 (v/v), sonicated for 10 min at 20°C, and centrifuged at 16,000*g* for 10 min. The supernatant was analyzed by ultra-performance liquid chromatography (UPLC)/electrospray ionization (ESI)-QTOFMS in positive and negative ion mode using method 1. Five individual plants were processed for each experimental condition.

Identification of Aglycones from Glycosylated Indole Derivatives

Six-week-old, $AgNO_3$-sprayed (5 mM, 24-h treatment) Col-0 leaves (1.5 g) were extracted twice with a total of 6 mL of methanol:water, 80:20 (v/v). The methanolic extract was evaporated to dryness in a vacuum centrifuge at 30°C. The remaining residue was redissolved in 1 mL of water:formic acid, 99.9:0.1 (v/v), sonicated for 10 min at 20°C, and centrifuged at 16,000*g* for 10 min. The supernatant was fractionated by preparative HPLC (YMC ODS-A; 150- × 20-mm; pore size, 120 Å; particle size, 5 μm; flow rate, 10 mL min^{-1}; gradient program: 0–1 min, isocratic, 95% A [water:formic acid, 99.9:0.1 {v/v}], 5% B [acetonitrile:formic acid, 99.9:0.1 {v/v}]; 1–31 min, linear from 5% B to 20% B; injection volume, 500 μL; fraction size, 10 mL). Fractions were evaporated to dryness in a vacuum centrifuge at 30°C, redissolved in 500 μL of water, and screened for glycosylated indole derivatives by UPLC/ESI-QTOFMS in negative ion mode using method 1. Aliquots of respective fractions were digested with β-glucosidase in sodium acetate buffer (for procedure, see below). Released aglycones were repeatedly extracted from the acidified aqueous layer with ethyl acetate. The combined ethyl acetate extracts were evaporated to dryness in a vacuum centrifuge at 30°C, reconstituted in 50 μL of methanol:water, 30:70 (v/v), and analyzed by UPLC/ESI-QTOFMS using method 2. Aglycones were identified by comparison of retention times and mass spectral data in relation to authenticated standards.

Determination of the Total Content of Substituted ICHO/ICOOH after β-Glucosidase Treatment

Ground leaf material (100 ± 5 mg) was spiked with 1 nmol of 5-MeO-ICHO as an internal standard and extracted twice with 200 μL of methanol:water, 80:20 (v/v) as described previously (Böttcher et al., 2009). The combined extracts were evaporated to dryness in a vacuum centrifuge at 30°C. To the remaining residue, 200 μL of sodium acetate buffer (50 mM, pH 5.0, adjusted with HCl) was added, and the mixture was sonicated for 10 min at 20°C. For enzymatic deglucosylation, the mixture was incubated with 2 units of β-glucosidase (EC 3.2.1.21; Sigma-Aldrich) under continuous shaking at 37°C for 2 h. After acidification with 100 μL of HCl (1 M), the mixture was repeatedly extracted with 3 × 100 μL of ethyl acetate. The combined organic extracts were evaporated to dryness in a vacuum centrifuge at 30°C. The remaining residue was reconstituted in 100 μL of methanol: water, 30:70 (v/v), sonicated for 10 min at 20°C, and centrifuged at 16,000*g* for 10 min. The supernatant was analyzed by UPLC/ESI-QTOFMS using method 2.

Relative response factors (RRFs) of individual target compounds in comparison with the internal standard 5-MeO-ICHO were obtained by analysis of dilution series prepared from the pure reference compounds in methanol: water, 30:70 (v/v). For quantification, extracted ion chromatograms (mass-to-charge ratio [*m/z*] width ± 0.02) of corresponding protonated molecular ions were integrated: ICOOH (retention time [t_r] 308 s, *m/z* 162.06, RRF 0.28), ICOOMe (t_r 422 s, *m/z* 176.07, RRF 0.57), 5-HO-ICOOH (retention time [t_r] 190 s, *m/z* 178.05, RRF 0.16), 6-HO-ICOOH (t_r 198 s, *m/z* 178.05, RRF 0.13), ICHO (t_r 305 s, *m/z* 146.06, RRF 0.77), 4-HO-ICHO (t_r 331 s, *m/z* 162.06, RRF 0.45), 5-HO-ICHO (t_r 194 s, *m/z* 162.06, RRF 0.32), 6-HO-ICHO (t_r 208 s, *m/z* 162.06, RRF 0.38), 4-methoxyindole-3-carbaldehyde (t_r 349 s, *m/z* 176.07, RRF 1.18), 5-MeO-ICHO (t_r 315 s, *m/z* 176.07, RRF 1.00), and camalexin (t_r 423 s, *m/z* 201.05, RRF 3.24).

Profiling of Indole Derivatives in Wild-Type and Mutant Plants

Wild-type, knockout, and overexpression plants (20 plants per genotype) were grown in parallel for 6 weeks. One hour after the beginning of the photoperiod, half of the plants was sprayed with 5 mM $AgNO_3$ whereas the other half remained without any treatment. After 24 h, rosette leaves of eight to nine uniform plants per genotype and treatment were harvested, individually pooled for each plant, and frozen and homogenized in liquid nitrogen. Ground leaf material (100 ± 5 mg) was extracted twice with 200 μL of methanol:water, 80:20 (v/v) as described previously (Böttcher et al., 2009). The combined extracts were evaporated to dryness in a vacuum centrifuge at 30°C. The remaining residue was reconstituted in 200 μL of methanol:water, 30:70 (v/v), sonicated for 10 min at 20°C, and centrifuged at 16,000*g* for 10 min. The supernatant was analyzed by UPLC/ESI-QTOFMS in negative ion mode using method 1. For relative quantification of indole derivatives, extracted ion chromatograms (*m/z* width ± 0.02) using quantifier ions/retention times from Table I were integrated. Two independent replicate experiments were performed, resulting in a total of 16 to 18 individual plants per genotype and treatment.

Quantification of Cell Wall-Bound ICOOH

Ground leaf material (approximately 150 mg) was sequentially extracted under sonication for 15 min at 40°C with 2 × 600 μL of methanol:water, 50:50 (v/v), 2 × 600 μL of methanol, and 2 × 600 μL of acetone. The remaining residue was dried at 30°C in a vacuum centrifuge and precisely weighed into a 2-mL polypropylene tube. Alkaline hydrolysis of cell wall material (5–7 mg per sample) was performed after the addition of 500 μL of NaOH (1 M; thoroughly degassed with N_2) and 5 μL of ascorbic acid (10%, w/v) for 20 h at 70°C under continuous shaking. After acidification with 60 μL of HCl (37%, w/v), the mixture was extracted with 3 × 400 μL of ethyl acetate. The combined organic extracts were evaporated to dryness in a vacuum centrifuge at 30°C. The remaining residue was reconstituted in 60 μL of methanol:water, 30:70 (v/v), sonicated for 10 min at 20°C, and centrifuged at 16,000*g* for 10 min. The supernatant was analyzed by UPLC/photodiode array/ESI-QTOFMS in negative ion mode using method 1. ICOOH was identified by mass spectrometry and quantified by integration of the UV chromatogram at 281 nm using an external calibration.

UPLC/ESI-QTOFMS

Method 1. Chromatographic separations were performed at 40°C on an Acquity UPLC system (Waters) equipped with an HSS T3 column (100 ×

1 mm, particle size 1.8 μm; Waters) applying the following binary gradient at a flow rate of 150 μL min^{-1}: 0 to 1 min, isocratic 95% A (water:formic acid, 99.9:0.1 [v/v]), 5% B (acetonitrile:formic acid, 99.9:0.1 [v/v]); 1 to 10 min, linear from 5% to 60% B; 10 to 12 min, isocratic 95% B; 12 to 14 min, isocratic 5% B. The injection volume was 2.6 μL (full loop injection). Eluted compounds were detected from *m/z* 100 to 1,000 using a MicrOTOF-Q hybrid QTOFMS (Bruker Daltonics) equipped with an Apollo II electrospray ion source in positive (negative) ion mode. The following instrument settings were applied: nebulizer gas, nitrogen, 1.6 bar; dry gas, nitrogen, 6 L min^{-1}, 190°C; capillary, −5,000 V (+4,000 V); end plate offset, −500 V; funnel 1 radio frequency (RF), 200 Volts peak-to-peak (Vpp); funnel 2 RF, 200 Vpp; in-source collision-induced dissociation (CID) energy, 0 V; hexapole RF, 100 Vpp; quadrupole ion energy, 3 eV; collision gas, argon; collision energy, 3 eV (10 eV); collision RF, 200/400 Vpp (timing 50/50); transfer time, 70 μs; prepulse storage, 5 μs; pulser frequency, 10 kHz; and spectra rate, 3 Hz.

Method 2. Chromatographic separations were performed at 50°C on an Acquity UPLC system equipped with a BEH Shield RP18 column (150 × 1 mm, particle size 1.7 μm; Waters) applying the same binary gradient as described above but using a flow rate of 140 μL min^{-1}. The injection volume was 2.6 μL (full loop injection). Eluted compounds were detected from *m/z* 75 to 700 using a MicrOTOF-Q in positive ion mode. Instrument settings were as described above for positive ion mode with the exception of one parameter: collision RF, 150/200 Vpp (timing 50/50).

Mass spectra were acquired in centroid mode. Calibration of the *m/z* scale was performed for individual raw data files on lithium formate cluster ions obtained by automatic infusion of 20 μL of 10 mM lithium hydroxide in isopropanol:water:formic acid, 49.9:49.9:0.2 (v/v/v) at the end of the gradient using a diverter valve. CID mass spectra were acquired as described previously (Böttcher et al., 2009). Putative elemental compositions were determined on the basis of accurate mass and isotope pattern matching using the SmartFormula algorithm implemented in DataAnalysis 4.0 (Bruker Daltonics) and checked for consistency in relation to elemental compositions calculated for fragment ions and neutral losses from respective CID mass spectra.

Establishment of 35S:AAO1, 35S:CYP71B6, and T-DNA Insertion Lines

The *AAO1* complementary DNA (cDNA) clone was kindly provided by Tomokazu Koshiba and Mitsunori Seo. *AAO1* and *CYP71B6* coding sequences were amplified from the cDNA clone and yeast expression plasmid (see below), respectively, using the primer pairs 5′-GGCTTAAUATGTCTCTTTTCTCCTTCCC-3′/5′-GGTTTAAUCTAAAGCTTGCGGTTGATGA-3′ and 5′-GGCTTAAUATGGGTGAGAAAGCGATTGAC-3′/5′-GGTTTAAUTCAAACATTTTTCCTTTGCTGG-3′, respectively, and cloned into pCAMBIA330035Su via USER technology (Nour-Eldin et al., 2006). *Agrobacterium tumefaciens*-mediated transformation of Arabidopsis Col-0 plants was performed via the floral dip method, and primary transformants were confirmed by BASTA resistance of the seedlings and by PCR analysis. Homozygous T4 plants were used for metabolite profiling.

For *AAO1*, the T-DNA insertion line SALK_069221 (third exon; in this article referred to as *aao1*), and for *CYP71B6*, the insertion lines GABI305A04 (*cyp71B6-1*; first exon) and SALK_115336 (*cyp71B6-2*; 3′ untranslated region), were confirmed and homozygous plants were identified by PCR. These lines were analyzed for transcript levels of *AAO1* and *CYP71B6*, respectively (Supplemental Fig. S3), which were strongly reduced in *aao1* and *cyp71B6-1*. In *cyp71B6-2*, only partial reduction of the transcript level was observed.

Expression Analysis

RNA extraction and cDNA synthesis have been described by Schuhegger et al. (2007). Quantitative real-time PCR was performed with the CyberGreen/Light Cycler system (Roche) using the following primers: *AAO1*, 5′-CCCGGGTATAGATCAAGCTTGGC-3′/5′-CCGCACAATGAGTGACTTCTTCT-3′; *CYP71B6*, 5′-GTGATCGGAAAATTCGCGGC-3′/5′-GCCATTGTCCAATCCAAAGT-3′; *ACTIN1*, 5′-TGGAACTGGAATGGTTAAGGCTGG-3′/5′-TCTCCAGAGTCGAGCACAATACCG-3′.

Aldehyde Oxidase Activity in Plants

Arabidopsis leaf material (2 g) was extracted in 10 mL of protein extraction buffer 1 (50 mM Tris, 1 mM EDTA, 1 μM sodium molybdate, 10 μM FAD, and 2 mM dithiothreitol, pH 7.5), adding 0.2 g g^{-1} fresh weight Polyclar-AT (Serva), and centrifuged at 17,400*g* for 15 min at 4°C. Ammonium sulfate was slowly added to the supernatant to a final concentration of 70% (4.28 g). After 1 h of stirring at 4°C and centrifuging at 17,400*g* for 10 min, the pellet was redissolved in 1 mL of protein extraction buffer 2 (20 mM Tris, 1 mM EDTA, 1 μM sodium molybdate, 10 μM FAD, and 2 mM dithiothreitol, pH 7.5), desalted using an NAP-10 column (GE Healthcare), and eluted in 1.5 mL of protein extraction buffer 2. Protein concentration was determined via Bio-Rad protein assay, 1.4 mg of protein was incubated with 125 μM ICHO for 30 min at 25°C in the same buffer, and the reaction was stopped by the addition of methanol (2 volumes) and analyzed by reverse-phase HPLC (LiChroCART 250-4, RP-18, 5 μm, Merck; flow rate, 1 mL min^{-1}; gradient: 0–2 min, isocratic, 20% A [water:formic acid, 99.7:0.3 {v/v}], 20% B [acetonitrile]; 2–12 min, linear from 20% to 38% B; 12–13 min, linear from 38% to 100% B; 13–15 min, isocratic, 100% B) equipped with a photodiode array detector (Dionex). The product peaks were identified and quantified by comparison with authentic standards: ICOOH, t_r = 10.8 min, absorption maximum (λ_{Max}) = 281 nm; ICHO, t_r = 11.4 min, λ_{Max} = 297 nm. Boiled protein sample was provided as a negative control.

Yeast Expression of CYP71B6

The CYP71B6 coding sequence was amplified from total Arabidopsis Col-0 leaf cDNA using the primers 5′-GGATTAAUAATGTCTTTGTTCTCTTTCCCAATTTCCACTGAG-3′/5′-GGGTTAAUTTAAAGCTTGCGGTTGATGACATT-3′, cloned into pYEDP60u via USER technology (Nour-Eldin et al., 2006), and transformed into *Saccharomyces cerevisiae* WAT11 (Pompon et al., 1996). Yeast microsomes were prepared as described by Schuhegger et al. (2006). Cyanide derivatization and HPLC analysis were performed as described previously (Böttcher et al., 2009). The concentration of active P450 was determined by carbon monoxide differential spectroscopy (Omura and Sato, 1964). For analysis of the enzymatic parameters, reactions were performed in 1 mL of potassium phosphate buffer (20 mM, pH 7.5) for 20 min. The reactions were stopped by the addition of 800 μL of methanol, dried in vacuum, and redissolved in 200 μL of methanol:water, 4:1 (v/v). IAN, ICHO, and ICOOH were analyzed by reverse-phase HPLC (MultoHigh 100 RP18-5μ, Göhler Analytik; flow rate, 1 mL min^{-1}; gradient: 0–2 min, isocratic, 20% A [water:formic acid, 99.7:0.3 {v/v}], 20% B [acetonitrile]; 2–12 min, linear from 20% to 28% B; 12–19 min, linear from 28% to 50% B; 19–22 min, linear from 50% to 100% B; 22–24 min, isocratic, 100% B), equipped with a photodiode array detector (Dionex). Quantification was based on calibration curves with authentic standards: ICOOH, t_r = 14.7 min; ICHO, t_r = 15.7 min; IAN, t_r = 22.0 min; λ_{Max} = 278 nm.

Accession numbers are as follows: AAO1, At5g20960; CYP71B6, At2g24180.

Supplemental Data

The following materials are available in the online version of this article.

Supplemental Figure S1. Identification of molecular features associated with ICHO/ICOOH derivatives whose accumulation depends on CYP79B2/B3 by combining chemical complementation of *cyp79B2 cyp79B3* and nontargeted UPLC/ESI-QTOFMS-based metabolite profiling.

Supplemental Figure S2. Enzymatic parameters of CYP71B6.

Supplemental Figure S3. *AAO1* and *CYP71B6* transcript abundance in corresponding T-DNA insertion lines.

Supplemental Figure S4. In vitro oxidation of ICHO.

Supplemental Figure S5. Quantification of cell wall-bound ICOOH in rosette leaves of nontreated (gray bars) and $AgNO_3$-treated (24 h after treatment; black bars) wild-type (Col-0) and mutant plants.

Supplemental Table S1. CID mass spectral data of identified ICHO/ICOOH derivatives.

Supplemental Table S2. Comprehensive coexpression analysis of AAO1 and CYP71B6, applying the ATTED-II platform.

Supplemental Table S3. Relative quantification of ICHO/ICOOH derivatives in nontreated leaves of wild-type and mutant/overexpressor plants nontreated and 24 h after $AgNO_3$ treatment.

Supplemental Table S4. Relative quantification of ICHO/ICOOH derivatives, statistical analysis.

Supplemental Table S5. Relative quantification of ICHO/ICOOH derivatives and camalexin 24 h after spraying 5 mM $AgNO_3$, statistical analysis.

ACKNOWLEDGMENTS

We thank Alfons Gierl for support, Tomokazu Koshiba and Mitsunori Seo (Tokyo Metropolitan University/RIKEN Plant Science Center) for providing the *AAO1* cDNA clone, Majse Nafisi (Copenhagen University) for providing *cyp71B6-1* seeds, Barbara Halkier (Copenhagen University) for helpful discussions and providing pCAMBIA330035Su, Beiying Dai (Technische Universität München) for generating *CYP71B6* primary transformants, Cornelia Götz (Technische Universität München) for the preparation of yeast microsomes, and Heidi Miller-Mommerskamp (Technische Universität München) for propagating plant lines.

Received January 16, 2014; accepted April 8, 2014; published April 11, 2014.

LITERATURE CITED

Agerbirk N, De Vos M, Kim JH, Jander G (2009) Indole glucosinolate breakdown and its biological effects. Phytochem Rev **8:** 101–120

Akaba S, Seo M, Dohmae N, Takio K, Sekimoto H, Kamiya Y, Furuya N, Komano T, Koshiba T (1999) Production of homo- and hetero-dimeric isozymes from two aldehyde oxidase genes of Arabidopsis thaliana. J Biochem **126:** 395–401

Bednarek P, Pislewska-Bednarek M, Svatos A, Schneider B, Doubsky J, Mansurova M, Humphry M, Consonni C, Panstruga R, Sanchez-Vallet A, et al (2009) A glucosinolate metabolism pathway in living plant cells mediates broad-spectrum antifungal defense. Science **323:** 101–106

Bednarek P, Piślewska-Bednarek M, Ver Loren van Themaat E, Maddula RK, Svatoš A, Schulze-Lefert P (2011) Conservation and clade-specific diversification of pathogen-inducible tryptophan and indole glucosinolate metabolism in Arabidopsis thaliana relatives. New Phytol **192:** 713–726

Bednarek P, Schneider B, Svatos A, Oldham NJ, Hahlbrock K (2005) Structural complexity, differential response to infection, and tissue specificity of indolic and phenylpropanoid secondary metabolism in Arabidopsis roots. Plant Physiol **138:** 1058–1070

Böttcher C, Westphal L, Schmotz C, Prade E, Scheel D, Glawischnig E (2009) The multifunctional enzyme CYP71B15 (PHYTOALEXIN DEFICIENT3) converts cysteine-indole-3-acetonitrile to camalexin in the indole-3-acetonitrile metabolic network of *Arabidopsis thaliana*. Plant Cell **21:** 1830–1845

Boyes DC, Zayed AM, Ascenzi R, McCaskill AJ, Hoffman NE, Davis KR, Görlach J (2001) Growth stage-based phenotypic analysis of *Arabidopsis*: a model for high throughput functional genomics in plants. Plant Cell **13:** 1499–1510

Clay NK, Adio AM, Denoux C, Jander G, Ausubel FM (2009) Glucosinolate metabolites required for an Arabidopsis innate immune response. Science **323:** 95–101

Denby KJ, Kumar P, Kliebenstein DJ (2004) Identification of Botrytis cinerea susceptibility loci in Arabidopsis thaliana. Plant J **38:** 473–486

Forcat S, Bennett M, Grant M, Mansfield JW (2010) Rapid linkage of indole carboxylic acid to the plant cell wall identified as a component of basal defence in Arabidopsis against hrp mutant bacteria. Phytochemistry **71:** 870–876

Gamir J, Pastor V, Cerezo M, Flors V (2012) Identification of indole-3-carboxylic acid as mediator of priming against Plectosphaerella cucumerina. Plant Physiol Biochem **61:** 169–179

García I, Rosas T, Bejarano ER, Gotor C, Romero LC (2013) Transient transcriptional regulation of the *CYS-C1* gene and cyanide accumulation upon pathogen infection in the plant immune response. Plant Physiol **162:** 2015–2027

Geu-Flores F, Møldrup ME, Böttcher C, Olsen CE, Scheel D, Halkier BA (2011) Cytosolic γ-glutamyl peptidases process glutathione conjugates in the biosynthesis of glucosinolates and camalexin in *Arabidopsis*. Plant Cell **23:** 2456–2469

Geu-Flores F, Nielsen MT, Nafisi M, Møldrup ME, Olsen CE, Motawia MS, Halkier BA (2009) Glucosinolate engineering identifies a gamma-glutamyl peptidase. Nat Chem Biol **5:** 575–577

Glawischnig E, Grün S, Frey M, Gierl A (1999) Cytochrome P450 monooxygenases of DIBOA biosynthesis: specificity and conservation among grasses. Phytochemistry **50:** 925–930

Glawischnig E, Hansen BG, Olsen CE, Halkier BA (2004) Camalexin is synthesized from indole-3-acetaldoxime, a key branching point between primary and secondary metabolism in Arabidopsis. Proc Natl Acad Sci USA **101:** 8245–8250

Hagemeier J, Schneider B, Oldham NJ, Hahlbrock K (2001) Accumulation of soluble and wall-bound indolic metabolites in Arabidopsis thaliana leaves infected with virulent or avirulent Pseudomonas syringae pathovar tomato strains. Proc Natl Acad Sci USA **98:** 753–758

Hull AK, Vij R, Celenza JL (2000) Arabidopsis cytochrome P450s that catalyze the first step of tryptophan-dependent indole-3-acetic acid biosynthesis. Proc Natl Acad Sci USA **97:** 2379–2384

Ibdah M, Chen YT, Wilkerson CG, Pichersky E (2009) An aldehyde oxidase in developing seeds of Arabidopsis converts benzaldehyde to benzoic acid. Plant Physiol **150:** 416–423

Iven T, König S, Singh S, Braus-Stromeyer SA, Bischoff M, Tietze LF, Braus GH, Lipka V, Feussner I, Dröge-Laser W (2012) Transcriptional activation and production of tryptophan-derived secondary metabolites in Arabidopsis roots contributes to the defense against the fungal vascular pathogen Verticillium longisporum. Mol Plant **5:** 1389–1402

Kiss G, Neukomm H (1966) Über die Struktur des Ascorbigens. Helv Chim Acta **49:** 989–992

Klein AP, Anarat-Cappillino G, Sattely ES (2013) Minimum set of cytochromes P450 for reconstituting the biosynthesis of camalexin, a major Arabidopsis antibiotic. Angew Chem Int Ed Engl **52:** 13625–13628

Koiwai H, Akaba S, Seo M, Komano T, Koshiba T (2000) Functional expression of two Arabidopsis aldehyde oxidases in the yeast Pichia pastoris. J Biochem **127:** 659–664

Kriechbaumer V, Wang P, Hawes C, Abell BM (2012) Alternative splicing of the auxin biosynthesis gene YUCCA4 determines its subcellular compartmentation. Plant J **70:** 292–302

Mashiguchi K, Tanaka K, Sakai T, Sugawara S, Kawaide H, Natsume M, Hanada A, Yaeno T, Shirasu K, Yao H, et al (2011) The main auxin biosynthesis pathway in Arabidopsis. Proc Natl Acad Sci USA **108:** 18512–18517

Mendel RR, Hänsch R (2002) Molybdoenzymes and molybdenum cofactor in plants. J Exp Bot **53:** 1689–1698

Mikkelsen MD, Hansen CH, Wittstock U, Halkier BA (2000) Cytochrome P450 CYP79B2 from Arabidopsis catalyzes the conversion of tryptophan to indole-3-acetaldoxime, a precursor of indole glucosinolates and indole-3-acetic acid. J Biol Chem **275:** 33712–33717

Møldrup ME, Salomonsen B, Geu-Flores F, Olsen CE, Halkier BA (2013) De novo genetic engineering of the camalexin biosynthetic pathway. J Biotechnol **167:** 296–301

Nafisi M (2007) Camalexin biosynthesis: identification and characterisation of the oxime-metabolising enzyme. PhD thesis. University of Copenhagen, Copenhagen

Nafisi M, Goregaoker S, Botanga CJ, Glawischnig E, Olsen CE, Halkier BA, Glazebrook J (2007) *Arabidopsis* cytochrome P450 monooxygenase 71A13 catalyzes the conversion of indole-3-acetaldoxime in camalexin synthesis. Plant Cell **19:** 2039–2052

Nakajima E, Nakano H, Yamada K, Shigemori H, Hasegawa K (2002) Isolation and identification of lateral bud growth inhibitor, indole-3-aldehyde, involved in apical dominance of pea seedlings. Phytochemistry **61:** 863–865

Nour-Eldin HH, Hansen BG, Nørholm MH, Jensen JK, Halkier BA (2006) Advancing uracil-excision based cloning towards an ideal technique for cloning PCR fragments. Nucleic Acids Res **34:** e122

Obayashi T, Okamura Y, Ito S, Tadaka S, Aoki Y, Shirota M, Kinoshita K (2014) ATTED-II in 2014: evaluation of gene coexpression in agriculturally important plants. Plant Cell Physiol **55:** e6

Omura T, Sato R (1964) The carbon monoxide-binding pigment of liver microsomes. II. Solubilization, purification, and properties. J Biol Chem **239:** 2379–2385

Pedras MS, Nycholat CM, Montaut S, Xu Y, Khan AQ (2002) Chemical defenses of crucifers: elicitation and metabolism of phytoalexins and indole-3-acetonitrile in brown mustard and turnip. Phytochemistry **59:** 611–625

Pedras MS, Yaya EE, Glawischnig E (2011) The phytoalexins from cultivated and wild crucifers: chemistry and biology. Nat Prod Rep **28:** 1381–1405

Pfalz M, Vogel H, Kroymann J (2009) The gene controlling *the Indole Glucosinolate Modifier1* quantitative trait locus alters indole glucosinolate structures and aphid resistance in *Arabidopsis*. Plant Cell **21:** 985–999

Pompon D, Louerat B, Bronine A, Urban P (1996) Yeast expression of animal and plant P450s in optimized redox environments. Methods Enzymol **272:** 51–64

Rauhut T, Glawischnig E (2009) Evolution of camalexin and structurally related indolic compounds. Phytochemistry **70:** 1638–1644

Saga H, Ogawa T, Kai K, Suzuki H, Ogata Y, Sakurai N, Shibata D, Ohta D (2012) Identification and characterization of ANAC042, a transcription factor family gene involved in the regulation of camalexin biosynthesis in Arabidopsis. Mol Plant Microbe Interact **25:** 684–696

Sandberg G, Jensen E, Crozier A (1984) Analysis of 3-indole carboxylic acid in Pinus sylvestris needles. Phytochemistry **23:** 99–102

Schuhegger R, Nafisi M, Mansourova M, Petersen BL, Olsen CE, Svatos A, Halkier BA, Glawischnig E (2006) CYP71B15 (PAD3) catalyzes the final step in camalexin biosynthesis. Plant Physiol **141:** 1248–1254

Schuhegger R, Rauhut T, Glawischnig E (2007) Regulatory variability of camalexin biosynthesis. J Plant Physiol **164:** 636–644

Seo M, Akaba S, Oritani T, Delarue M, Bellini C, Caboche M, Koshiba T (1998) Higher activity of an aldehyde oxidase in the auxin-overproducing *superroot1* mutant of *Arabidopsis thaliana*. Plant Physiol **116:** 687–693

Seo M, Koiwai H, Akaba S, Komano T, Oritani T, Kamiya Y, Koshiba T (2000) Abscisic aldehyde oxidase in leaves of Arabidopsis thaliana. Plant J **23:** 481–488

Sibbesen O, Koch B, Halkier BA, Møller BL (1994) Isolation of the heme-thiolate enzyme cytochrome P-450TYR, which catalyzes the committed step in the biosynthesis of the cyanogenic glucoside dhurrin in Sorghum bicolor (L.) Moench. Proc Natl Acad Sci USA **91:** 9740–9744

Sønderby IE, Geu-Flores F, Halkier BA (2010) Biosynthesis of glucosinolates: gene discovery and beyond. Trends Plant Sci **15:** 283–290

Stepanova AN, Yun J, Robles LM, Novak O, He W, Guo H, Ljung K, Alonso JM (2011) The *Arabidopsis* YUCCA1 flavin monooxygenase functions in the indole-3-pyruvic acid branch of auxin biosynthesis. Plant Cell **23:** 3961–3973

Su T, Xu J, Li Y, Lei L, Zhao L, Yang H, Feng J, Liu G, Ren D (2011) Glutathione-indole-3-acetonitrile is required for camalexin biosynthesis in *Arabidopsis thaliana*. Plant Cell **23:** 364–380

Tan J, Bednarek P, Liu J, Schneider B, Svatos A, Hahlbrock K (2004) Universally occurring phenylpropanoid and species-specific indolic metabolites in infected and uninfected Arabidopsis thaliana roots and leaves. Phytochemistry **65:** 691–699

Toufighi K, Brady SM, Austin R, Ly E, Provart NJ (2005) The Botany Array Resource: e-northerns, expression angling, and promoter analyses. Plant J **43:** 153–163

Wang MY, Liu XT, Chen Y, Xu XJ, Yu B, Zhang SQ, Li Q, He ZH (2012) Arabidopsis acetyl-amido synthetase GH3.5 involvement in camalexin biosynthesis through conjugation of indole-3-carboxylic acid and cysteine and upregulation of camalexin biosynthesis genes. J Integr Plant Biol **54:** 471–485

Won C, Shen X, Mashiguchi K, Zheng Z, Dai X, Cheng Y, Kasahara H, Kamiya Y, Chory J, Zhao Y (2011) Conversion of tryptophan to indole-3-acetic acid by TRYPTOPHAN AMINOTRANSFERASES OF ARABIDOPSIS and YUCCAs in Arabidopsis. Proc Natl Acad Sci USA **108:** 18518–18523

Wu A, Allu AD, Garapati P, Siddiqui H, Dortay H, Zanor MI, Asensi-Fabado MA, Munné-Bosch S, Antonio C, Tohge T, et al (2012) *JUNGBRUNNEN1*, a reactive oxygen species-responsive NAC transcription factor, regulates longevity in *Arabidopsis*. Plant Cell **24:** 482–506

Zarepour M, Simon K, Wilch M, Nieländer U, Koshiba T, Seo M, Lindel T, Bittner F (2012) Identification of superoxide production by Arabidopsis thaliana aldehyde oxidases AAO1 and AAO3. Plant Mol Biol **80:** 659–671

Zhao Y, Hull AK, Gupta NR, Goss KA, Alonso J, Ecker JR, Normanly J, Chory J, Celenza JL (2002) Trp-dependent auxin biosynthesis in Arabidopsis: involvement of cytochrome P450s CYP79B2 and CYP79B3. Genes Dev **16:** 3100–3112

Zhou N, Tootle TL, Glazebrook J (1999) *Arabidopsis PAD3*, a gene required for camalexin biosynthesis, encodes a putative cytochrome P450 monooxygenase. Plant Cell **11:** 2419–2428